

Adaptive Cluster Expansion (ACE): A Multilayer Network for Estimating Probability Density Functions*

S P Luttrell

October 18, 2018

Abstract: We derive an adaptive hierarchical method of estimating high dimensional probability density functions. We call this method of density estimation the “adaptive cluster expansion”, or ACE for short. We present an application of this approach, based on a multilayer topographic mapping network, that adaptively estimates the joint probability density function of the pixel values of an image, and presents this result as a “probability image”. We apply this to the problem of identifying statistically anomalous regions in otherwise statistically homogeneous images.

1 Introduction

The purpose of this paper is to develop a novel type of adaptive network for estimating probability density functions (PDF) for use in Bayesian analysis [1, 2]. We consider only techniques that scale well for use in high dimensional spaces, such as the analysis of large arrays of pixels in image processing. There are many attempts to solve this type of density estimation problem. For instance, the Boltzmann machine [3] is essentially a trainable Gibbs distribution, which permits arbitrarily complicated statistical structure to be modelled via hidden variables. Unfortunately, this generality must be paid for by performing lengthy Monte Carlo simulations. There are various extensions to this technique, such as the higher order Boltzmann machine [4], which capture higher order statistical behaviour more economically, but none of these variations has been shown to be suitable for high-dimensional image processing problems. Using maximum entropy techniques [5], we develop a number of variations on the Gibbs distribution approach [6], and propose a scheme in which we replace simple interactions between a large number of hidden variables (as in the Boltzmann machine) by complicated interactions which directly model the statistical structure of the data; this is an extreme form of the approach taken in [4].

The novel adaptive density estimator that we develop in [6] is based on a multilayer network, in which we choose the layer-to-layer connections to be hierarchical, and the layer-to-layer transformations to be topographic mappings [7]; this adaptively transforms the input data into a multiscale “pyramid-like”

*This paper was submitted to IEEE Trans. NN on 16 December 1991. Paper TNN #1115. It was not accepted for publication, but it underpins several subsequently published papers.

format. In [6] we further propose that the joint PDFs of adjacent nodes in each layer should be combined to form an estimate of the joint PDF of the nodes in the input layer. By analogy with the standard derivation of Gibbs distributions, we can also derive our joint PDF estimate by applying the maximum entropy method [5]. However, our result is computationally much cheaper to implement than a standard Gibbs distribution, because we do not need to perform Monte Carlo simulations in order to integrate over the states of hidden variables. We suggest the name “adaptive cluster expansion” (ACE) for this type of network estimate of high-dimensional joint PDFs. Other literature on this approach can be found in [8, 9, 10, 11, 12], where we further develop multilayer topographic mapping networks, and their relationship to vector quantisers.

The purpose of this paper is to present a complete account of ACE, and to demonstrate its effectiveness when applied to the problem of density estimation. We do not dwell on the details of how to implement the topographic mapping training algorithm (we review this in the appendix). In Section 2 we develop the ACE method of density estimation by appealing to simple counting arguments. In Section 3 we demonstrate the power of ACE by applying it to the problem of estimating the joint PDF of the pixels of textured images selected from the Brodatz album [13].

2 Probability Density Function Estimation

In this section we present a derivation of the ACE estimate $Q(\mathbf{x})$ of a PDF $P(\mathbf{x})$. We develop this result by appealing to simple counting arguments and by using a diagrammatic language.

2.1 Derivation of the ACE Estimate of a PDF

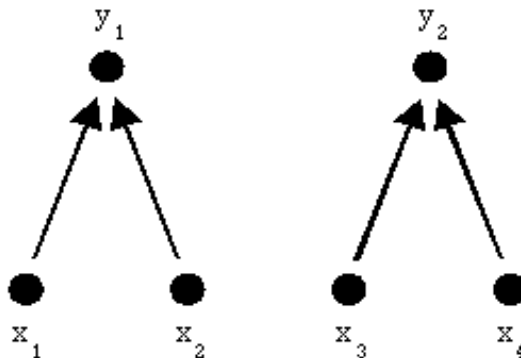


Figure 1: Basic 2-layer network. The input space (layer 0) is 4-dimensional and the output space (layer 1) is 2-dimensional. The layer 0-to-1 transformation factorises into two independent transformations: y_1 depends only on (x_1, x_2) , and y_2 depends only on (x_3, x_4) .

We show a simple network in Figure 1, where the input space is 4-dimensional, the output space is 2-dimensional, and we factorise the feedforward transforma-

tion as $\mathbf{y}(\mathbf{x}) = (y_1(x_1, x_2), y_2(x_3, x_4))$. Suppose we estimate the joint PDF $P_{\text{out}}(y_1, y_2)$ of the outputs, and the joint PDFs $P_{\text{in},12}(x_1, x_2)$ and $P_{\text{in},34}(x_3, x_4)$ of each pair of inputs, by measuring their histograms, for instance. Using this information alone we now wish to construct an estimate $Q(\mathbf{x})$ of the true joint PDF $P(\mathbf{x})$ of the 4-dimensional input. There are two alternative, but equivalent, ways of writing $Q(\mathbf{x})$, each of which has its own interesting interpretation.

Firstly, we may write

$$Q(\mathbf{x}) = P_{\text{out}}(y_1(x_1, x_2), y_2(x_3, x_4)) \frac{P_{\text{in},12}(x_1, x_2)}{P_{\text{out}}(y_1(x_1, x_2))} \frac{P_{\text{in},34}(x_3, x_4)}{P_{\text{out}}(y_2(x_3, x_4))} \quad (1)$$

In Equation 1 we construct $Q(\mathbf{x})$ as follows. We use $P_{\text{out}}(y_1, y_2)$ directly to estimate the joint PDF of the outputs, and indirectly to estimate the joint PDF of the inputs. In order to convert a PDF in output space (i.e. $P_{\text{out}}(y_1, y_2)$) into a PDF in input space we must divide $P_{\text{out}}(y_1, y_2)$ by a compression factor equal to the number of input values that can produce the observed output value. Because we obtain y_1 and y_2 *separately* from the pairs (x_1, x_2) and (x_3, x_4) , respectively, this compression factor is the product of two separate factors. For instance, the compression factor corresponding to y_1 is the ratio $\frac{P_{\text{out}}(y_1(x_1, x_2))}{\langle P_{\text{in},12}(x_1, x_2) \rangle}$, where $\langle P_{\text{in},12}(x_1, x_2) \rangle$ is the average value of $P_{\text{in},12}(x_1, x_2)$ over all the (x_1, x_2) that produce the same value of y_1 . However, we may refine this compression factor by using $P_{\text{in},12}(x_1, x_2)$ instead of $\langle P_{\text{in},12}(x_1, x_2) \rangle$ in the denominator, to yield the ratio $\frac{P_{\text{out}}(y_1(x_1, x_2))}{P_{\text{in},12}(x_1, x_2)}$. An analogous argument may be applied to obtain the compression factor corresponding to y_2 , and the results combined to obtain the final expression for $Q(\mathbf{x})$ as shown in Equation 1.

$$Q(\mathbf{x}) = P_{\text{in},12}(x_1, x_2) P_{\text{in},34}(x_3, x_4) \frac{P_{\text{out}}(y_1(x_1, x_2), y_2(x_3, x_4))}{P_{\text{out}}(y_1(x_1, x_2)) P_{\text{out}}(y_2(x_3, x_4))} \quad (2)$$

which is trivially the same as Equation 1, but we have arranged its terms in a new way. This furnishes us with an alternative interpretation of $Q(\mathbf{x})$. Thus, imagine that we are provided only with $P_{\text{in},12}(x_1, x_2)$ and $P_{\text{in},34}(x_3, x_4)$, and no information about the correlations between the pair (x_1, x_2) and the pair (x_3, x_4) . This is sufficient for us to construct $Q(\mathbf{x})$ as the product $P_{\text{in},12}(x_1, x_2) P_{\text{in},34}(x_3, x_4)$. Now, we admit that in fact we also know $P_{\text{out}}(y_1, y_2)$, which is a source of information about correlations between the pair (x_1, x_2) and the pair (x_3, x_4) . We make use of this information by forming the dimensionless ratio $\frac{P_{\text{out}}(y_1, y_2)}{P_{\text{out}}(y_1) P_{\text{out}}(y_2)}$, which differs from unity when y_1 and y_2 are correlated random variables (i.e. $P_{\text{out}}(y_1, y_2) \neq P_{\text{out}}(y_1) P_{\text{out}}(y_2)$). This ratio is greater (or less) than unity when the pair (y_1, y_2) is more (or less) likely to occur than would have been estimated from knowledge of the marginal PDFs $P_{\text{out}}(y_1)$ and $P_{\text{out}}(y_2)$ alone. Finally, we use this dimensionless ratio as a correction factor to obtain the expression for $Q(\mathbf{x})$ shown in Equation 2. This derivation is heuristic, but it leads to the same result as shown in Equation 1.

In Figure 2 we present an alternative representation of the network in Figure 1, in which we emphasise the PDFs that we use to construct $Q(\mathbf{x})$. Thus we introduce a shorthand notation in which we use an oval to highlight each clique of nodes in the network. We define the word ‘‘clique’’ to mean ‘‘complete set of nodes having the same parent node’’. As is conventional when discussing tree-like networks, we regard the higher layers of the network as being the ancestors

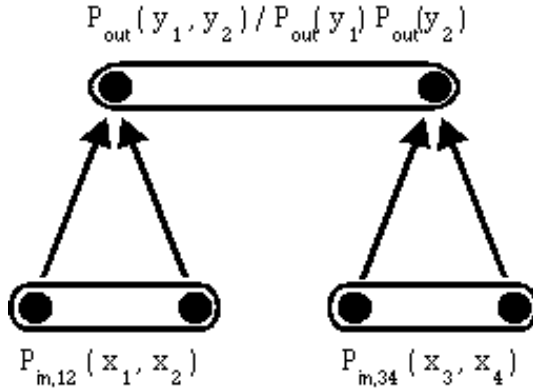


Figure 2: The clique PDFs that we use in the basic 2-layer network. $P_{\text{out}}(y_1, y_2)$ is the joint PDF of the pair of network outputs, and $P_{\text{out}}(y_1)$ and $P_{\text{out}}(y_2)$ are its two marginal PDFs. $\frac{P_{\text{out}}(y_1, y_2)}{P_{\text{out}}(y_1) P_{\text{out}}(y_2)}$ is a dimensionless ratio which records correlations between y_1 and y_2 . $P_{\text{in},12}(x_1, x_2)$ and $P_{\text{in},34}(x_3, x_4)$ are the joint PDFs of the pairs of inputs from which y_1 and y_2 derive, respectively.

of the lower layers, regardless of the fact that the direction of information flow is in the opposite direction through the tree. We then construct $Q(\mathbf{x})$ as the product of the three clique PDFs shown, whilst ensuring that the clique in layer 1 is appropriately normalised to render its contribution dimensionless. This leads to the form of $Q(\mathbf{x})$ in Equation 2.

This diagrammatic approach to constructing $Q(\mathbf{x})$ may be readily extended to any tree-like feedforward network. We favour this approach, because the basic strategy for deriving $Q(\mathbf{x})$ by invoking compression factors remains the same, but the burden of notational detail becomes somewhat heavy, so diagrams provide an ideal shortcut. For convenience, we summarise the prescription for constructing $Q(\mathbf{x})$ from a tree-like diagram as follows:

1. Estimate all of the clique PDFs, as histograms, for instance.
2. Deduce all of the single-node marginal PDFs from the clique PDFs estimated in the previous step. For instance this would create $P_{\text{out}}(y_1)$ and $P_{\text{out}}(y_2)$ from $P_{\text{out}}(y_1, y_2)$. This step is not needed in in layer 0.
3. From the results estimated in the previous two steps, for each clique compute a clique factor as follows:
 - (a) In the input layer the factor is the clique PDF itself.
 - (b) In other layers the factor is the clique PDF divided by the product of its marginal PDFs (e.g. $\frac{P_{\text{out}}(y_1, y_2)}{P_{\text{out}}(y_1) P_{\text{out}}(y_2)}$).
4. Finally, to construct $Q(\mathbf{x})$, form the product of all of the clique factors estimated in the previous step.

2.2 Translation Invariance

A disadvantage of the above prescription for constructing $Q(\mathbf{x})$ is that it does not treat the components of \mathbf{x} on an equal footing. For instance, in Equation 2 we see that the pair (x_1, x_2) is treated differently from the pair (x_2, x_3) , even though both of these are pairs of adjacent components in the data. In order to solve this problem we construct a number of different tree-like networks, each of which breaks symmetry in its own peculiar way, and then we combine the results from each network to construct a composite $Q(\mathbf{x})$ which respects the required symmetry.

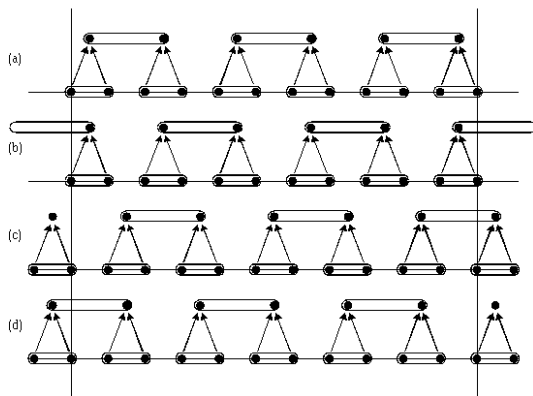


Figure 3: An example of the 4 separate 2-layer networks that we need to combine in order to produce a $Q(\mathbf{x})$ that treats each component of \mathbf{x} on an equal footing. Figure 3a shows the basic 2-layer network, Figure 3b shows the same network with the layer 1 clique PDFs translated. Figure 3c and Figure 3d derive from Figure 3a and Figure 3b by simultaneously translating the clique PDFs in both network layers.

In Figure 3 we show an example of the set of 4 different 2-layer networks which we need to combine in order to construct a composite $Q(\mathbf{x})$. In this example we assume that the input is a high dimensional vector, so we can ignore edge effects. We replicate the basic network structure of Figure 2 across the input vector, as shown. Each of the 4 networks has its own set of clique PDFs (drawn as ovals in Figure 2), each of which leads to its own estimate $Q(\mathbf{x})$ which breaks symmetry. However, a symmetric combination (such as the arithmetic or geometric mean) of these 4 results treats each component of \mathbf{x} on an equal footing. We can verify this by noting that the set of cliques that contributes in the spatial neighbourhood of each component of \mathbf{x} does not depend (apart from a trivial overall translation) on which component we select.

We must select a prescription for forming the composite $Q(\mathbf{x})$. It needs only to be a symmetric combination of the 4 individual estimates that we show in Figure 3; the arithmetic mean and geometric mean are obvious choices. On pragmatic grounds, we choose to use the geometric mean, because it corresponds to the arithmetic mean of $\log Q(\mathbf{x})$, which is more convenient to perform in limited precision hardware ($\log Q(\mathbf{x})$ has a much smaller dynamic range than $Q(\mathbf{x})$, assuming that we avoid the logarithmic singularity).

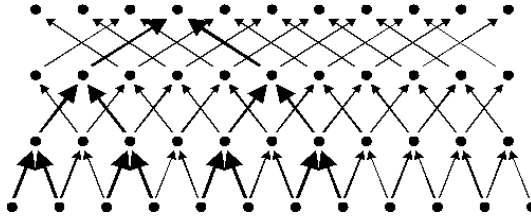


Figure 4: Example of the composite network connectivity that we require in order for a single network to compute a composite $Q(\mathbf{x})$, which treats each component of the input on an equal footing. This connectivity is the union of all of the binary trees can be generated from a reference binary tree (which we highlight in bold).

In Figure 4 we show the connectivity of part of a 4-layer composite network that can be used to process the input data in preparation for constructing a composite $Q(\mathbf{x})$. This connectivity contains all possible embedded tree-like networks, and in Figure 4 we highlight one such embedded tree for illustrative purposes.

For an n -layer network, we form the composite $Q(\mathbf{x})$ as the geometric mean over the $Q(\mathbf{x})$ derived from all tree-like networks that are embedded in this composite network, to yield the geometric mean PDF $Q_{\text{gm}}(\mathbf{x})$ in the form

$$\log Q_{\text{gm}}(\mathbf{x}) = \sum_{L=0}^{n-1} \frac{1}{2^{L+1}} \sum_k \log P_k^L \quad (3)$$

where L sums over layers 0 to $n-1$ of the network, k sums over cliques within a layer of the network, and P_k^L is the clique PDF at position k in layer L . It is important to note that the cliques are not simply adjacent nodes in each layer of the network. We must select pairs of nodes that form a “complete set of nodes having the same parent node”. In layer 0 this means that the nodes are adjacent. In layer 1 the nodes in a pair are separated by 1 intervening node. In layer 2 there are 3 intervening nodes, and so on. For $L \geq 1$ we must ensure that the P_k^L are dimensionless by dividing out the marginal PDFs, as in Equation 2. The $\frac{1}{2^{L+1}}$ factor ensures that we include each tree-like network exactly once, and that the final result is indeed the geometric mean of these contributions. Figure 3 shows the terms that Equation 3 generates when we set $n = 2$.

There are two further assumptions that we could make in order to simplify our result even further. Firstly, we could assume that the layer-to-layer transformations in Figure 4 were independent of position k within each layer L . Secondly, we could assume that the clique PDFs were independent of position k within each layer L . We can make both of these assumptions if the statistical properties of the input data are known to be translationally invariant (such as might be the case for an image of a texture, for instance). In all of our numerical simulations we make these two simplifying assumptions.

2.3 Modular Implementation

We now describe a practical implementation of Equation 3 in the context of image processing (i.e. 2-dimensional arrays of pixels of data). There are three basic

operations to perform. We must use a training set to determine suitable layer-to-layer transformations, then estimate the clique PDFs in each network layer, and then construct $\log Q_{\text{gm}}(\mathbf{x})$ from these estimates. Ideally we should optimise the layer-to-layer transformations directly so that the constructed $Q_{\text{gm}}(\mathbf{x})$ is “close to” $P(\mathbf{x})$ in some sense (e.g. relative entropy), but we have not yet found a computationally cheap way of doing this. Instead, we tackle the problem indirectly, by using our existing multilayer topographic mapping network technique [10]. There are two main reasons for this choice. Firstly, this type of network is computationally cheap to train; we typically train such a network at the rate of 2.3 second per layer on a VAXstation 3100 workstation (assuming 6 bit data values). Secondly, the network encodes the input in such a way as to be able to reconstruct it approximately from the state of any network layer. Although this second property does not in general imply that the encoded input is the optimal one for constructing an estimate of the input PDF, it turns out that it does produce useful results.

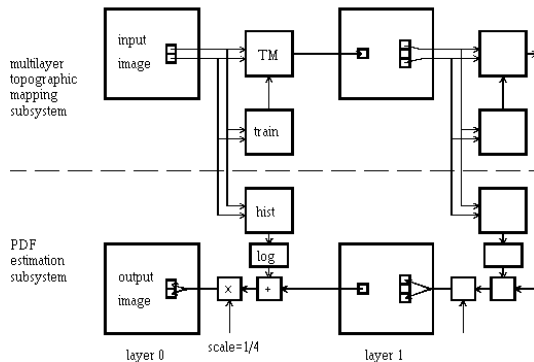


Figure 5: First two layers of a modular system for constructing $Q_{\text{gm}}(\mathbf{x})$. The top half of the diagram is a multilayer network subsystem (actually, a multilayer topographic mapping in this case), which operates from left to right. The bottom half of the diagram is the PDF estimation subsystem, which operates from right to left. We connect the two systems by feeding logarithmic clique PDFs measured in the multilayer network through to be added together in the PDF estimator.

In Figure 5 we show a system for constructing $Q_{\text{gm}}(\mathbf{x})$, which consists of two interconnected subsystems - a multilayer topographic mapping subsystem for transforming the input image, and a PDF estimation subsystem for forming an output image which contains the contributions to $Q_{\text{gm}}(\mathbf{x})$, each recorded in its spatially correct location in the image. For obvious reasons, we call the output image a “probability image”. The flow from left to right across the top half of Figure 5 implements the network structure in Figure 4, and the flow from right to left across the bottom half of Figure 5 progressively constructs the probability image.

In Figure 5 the input image becomes layer 0 of a multilayer network. In layer 0 we extract a pair of adjacent pixels, and then pass it through a look-up table (or mapping) to yield a single value which we write into the appropriate pixel location in layer 1 (in Figure 1 this corresponds to transforming (x_1, x_2)

to become y_1). We repeat this operation all over layer 0, to yield a whole array of transformed values in layer 1. There is an arbitrariness in our choice of the relative position of the pairs of pixels that we use (e.g. north-south, or east-west, etc). In our simulations we use a north-south relative position in the layer 0-to-1 transformation, east-west in the layer 1-to-2 transformation, and alternate these two choices thereafter as we progress from layer to layer of the network. Note also that the separation of the pairs of pixels is not the same in each layer. In Figure 4 the separation doubles as we progress from layer to layer, but in Figure 5 the separation doubles after every two layers, because we must allow both the east-west and the north-south orientations to be processed at all separations (this is a consequence of processing 2-dimensional data through a 1-dimensional tree-structured network). If we concentrate only on the topology of the network that results from this prescription in Figure 5, we discover that it is identical to the topology in Figure 4. Thus, the only difference between these two cases is the way in which we identify the pixels of the input data array with the layer 0 nodes.

We may use any transformation that we wish in the look-up table. We have not yet discovered a computationally cheap way of optimising the network in order to construct a $Q(\mathbf{x})$ that best approximates the required $P(\mathbf{x})$. Instead, we optimise the network in such a way that each layer could be used to reconstruct approximately the state of the previous layer. This is not the same optimisation problem, but it is computationally very cheap, and empirically it leads to useful results for $Q(\mathbf{x})$. We choose to train the network as a multilayer topographic mapping, which we implement in a look-up table after the training schedule has ended. Typically, the largest number of bits per pixel that we use is 8, which corresponds to a look-up table with 65536 ($= 2^{2 \times 8}$) separate addresses, each containing an 8 bit output value.

When we have trained a sufficient number of layers, we may estimate the clique PDFs in each layer. We simply record these as histograms, without making any attempt to interpolate or smooth these estimates; later on we shall mention a number of caveats. This completes the left-to-right pass in the top half of Figure 5.

In order to construct our geometric mean estimate $Q_{\text{gm}}(\mathbf{x})$ of $P(\mathbf{x})$, we must combine the estimates of the clique PDFs. We may obtain the result in Equation 3 by appropriately scaling and summing the logarithms of the histograms (and their marginal histograms) in Figure 5. The method that we use depends on the following rearrangement of Equation 3

$$\log Q_{\text{gm}}(\mathbf{x}) = \left(\cdots \left(\frac{1}{2} \sum_{k_{n-3}} \log P_{k_{n-3}}^{n-3} + \frac{1}{2} \left(\sum_{k_{n-2}} \log P_{k_{n-2}}^{n-2} + \frac{1}{2} \sum_{k_{n-1}} \log P_{k_{n-1}}^{n-1} \right) \right) \right) \quad (4)$$

in which we successively compute the contributions starting at network layer $n-1$, and then work outwards towards layer 0. First of all we initialise all of the images in the PDF estimation subsystem to some constant value (say zero), and then commence at layer $n-1$ (i.e. the righthandmost layer in Figure 5). Using the notation of Figure 2, each clique in the multilayer topographic mapping subsystem contributes a term of the form $\log P_{\text{out}}(y_1, y_2) - \log P_{\text{out}}(y_1) - \log P_{\text{out}}(y_2)$, which we add to the values stored in the two pixels that are located at the same clique position in the PDF estimation subsystem. In order to compensate for

this double counting, and in order to account for the $\frac{1}{2}$ factors that appear in Equation 4, we scale the logarithmic value by a factor $\frac{1}{4}$ ($= \frac{1}{2} \times \frac{1}{2}$). We then progress layer by layer towards the left in Figure 5. At each layer we generate its logarithmic contribution as above, but now we add to this the contribution from the layer on its right, as shown in Figure 5 and Equation 4. By cascading the results backwards from layer to layer of the network, we iteratively construct $\log Q_{\text{gm}}(\mathbf{x})$ in the form shown in Equation 4. Note that the layer 0 cliques are slightly different, because they contribute terms of the form $\log P_{\text{in},12}(x_1, x_2)$.

When all of these stages are complete, the output image in Figure 5 contains pixel values whose sum equals the required $\log Q_{\text{gm}}(\mathbf{x})$. The contribution to $\log Q_{\text{gm}}(\mathbf{x})$ that is recorded in an output pixel derives from a (rectangular) region in the input image that surrounds the location of the output pixel, so the output image can be interpreted as an image of correctly spatially registered logarithmic probability contributions to $\log Q_{\text{gm}}(\mathbf{x})$.

In our simulations we investigate how each individual layer of the multilayer network contributes to $\log Q_{\text{gm}}(\mathbf{x})$, so we switch off all except one of the sources of logarithmic probability in Figure 5, which permits only a single layer of the network to contribute to the construction of the output image. Because each layer of the network typically is sensitive to statistical structure in the input image at only one length scale, the output image then typically reveals contributions to $\log Q_{\text{gm}}(\mathbf{x})$ at only one length scale.

We should remark in passing that there are many other possible ways in which Figure 5 could be configured. Our results depend on an underlying tree-like structure, which we replicate to produce the translation invariant network in Figure 4, which we then use directly to produce the design in Figure 5. In the case of a non-binary tree we must be careful to produce the correct generalisation of Figure 4 and Figure 5, but there are no new difficulties in principle.

2.4 Algorithmic Details

We compensate for some of the effects of non-uniform illumination of the scene in the input image by adding a grey scale wedge whose gradient we choose in such a way as to remove the linear component of the non-uniformity. This improves the assumed translation invariance of the image statistics. We do not attempt to perform a histogram equalisation on the input image, because the transformation from network layer 0 to layer 1 tends to perform this function anyway. In order not to disrupt the discussion, we review the details of the topographic mapping training algorithm in the appendix.

We choose to process the image in alternate directions using the following sequence: north/south, east/west, north/south, east/west, etc. This sequence leads to the following sequence of rectangular regions of the input image that influence the value in each pixel in each layer of the network: 1×2 , 2×2 , 2×4 , 4×4 , etc, using (east/west, north/south) coordinates. In all of our experiments we use a 6-layer network, so the value in each pixel in the final layer is sensitive to an 8×8 region of the input image.

The number of bits per pixel B that we use in each layer of the network determines the quality of the topographic mappings (the B bit output from a topographic mapping is the index of the winner from amongst 2^B competing “neurons”). Increasing B improves the quality of the mapping but increases the training time; we need to compromise between these two conflicting require-

ments. In our work on simple Brodatz texture images we find that choosing B to lie between 6 and 8 proves to be sufficient. Note that we choose to use the same number of bits per pixel in each layer of the network. In general this restriction is not necessary.

It is important to note that for a given value of B there is an upper limit on the allowed entropy (per unit area) that the input data should have. A hierarchically connected multilayer topographic mapping network progressively squeezes the input data through an ever smaller bottleneck (in fact there are multiple parallel bottlenecks due to the overlapping tree structure) as we pass through the layers of the network. There is a upper limit to the number of network layers beyond which it simply cannot preserve information that is useful in estimating the joint density of the input data, which limits the capabilities of our current method.

The choice of the size of the histogram bins is also important. A property of the multilayer topographic mapping network is that adjacent histogram bins derive from input vectors that are close to each other (in the Euclidean sense), so it makes sense to rebin the histogram by adding together the contents of adjacent bins. We may easily control the histogram bin size by truncating the low order bits of each pixel value. If we truncate b low order bits of each pixel value, then effectively we smooth the histogram over 2^b adjacent bins (for each dimension of the histogram). As we smooth the histogram it will suffer from less noise, but we run the danger of smoothing away significant structure that might usefully be used to characterise the statistics of the input image; so we need to make a compromise.

It is most important not to use histogram bins that are too small. A large number of small histogram bins would record the details of the statistical fluctuations of the training image (as particular realisations of a Poisson noise process in each bin), and would act as a detailed record of the structure in the training image, and thus be unable to generalise very well. Such histograms would look very spiky, and in extreme cases there might be counts recorded in only a few bins, with zeros in all of the remaining bins. If this situation were to occur, then the training image would have a large $Q_{\text{gm}}(\mathbf{x})$, whereas a test image (having the same statistical properties) would have a small $Q_{\text{gm}}(\mathbf{x})$. The cause of this problem is the absence of a significant overlap between the spikes in the training and test image histograms, which could be avoided by ensuring that the histogram bins are not too small. Generally, we find that a little experimentation can be used to determine a robust histogram binning strategy, so we do not attempt to implement a more sophisticated technique here.

Finally, we display the contributions to $\log Q_{\text{gm}}(\mathbf{x})$ as follows. We determine the range of pixel values that occurs in the image, and we translate and scale this into the range $[0, 255]$. This ensures that the smallest logarithmic probability appears as black, and the largest logarithmic probability appears as white, and all other values are linearly scaled onto intermediate levels of grey. This prescription has its dangers because each image determines its own special scaling, so one should be careful when comparing two different images. It can also be adversely affected by pixel value outliers arising from Poisson noise effects, where an extreme value of a single pixel could affect the way in which the whole of an image is displayed. However, we find that the overlapping tree structure of our multilayer network causes enough averaging together of individual contributions $Q(\mathbf{x})$ that the composite result $Q_{\text{gm}}(\mathbf{x})$ does not suffer from problems

due to pixel value outliers.

3 Application to the Detection of Anomalies in Textures

In this section we present the results of applying the system shown in Figure 5 to four 256×256 images of textures taken from the Brodatz texture album [13]. In all cases we compensate for uneven illumination by introducing a grey scale wedge as we explained earlier, we use 8 bits per pixel for the topographic mappings, we use 6 bits per pixel for histogramming, and we invert the $[0, 255]$ scale to represent the contributions to $\log Q_{\text{gm}}(\mathbf{x})$ in such a way that white pixels indicate a small (rather than a large) contribution to $\log Q_{\text{gm}}(\mathbf{x})$. Thus white pixels in the output image correspond to regions of the input image whose statistical properties differ markedly from the statistics averaged over the whole image. We usually call this representation of the contributions to $\log Q_{\text{gm}}(\mathbf{x})$ an “anomaly image”.

We do not present these results as necessarily being an efficient way of detecting texture anomalies. Rather, we merely apply our novel method of estimating PDFs, as expressed in Equation 3 and in Figure 5, to the particular problem of texture analysis, because this is an effective way of demonstrating some of the more interesting properties of $\log Q_{\text{gm}}(\mathbf{x})$.

3.1 Texture 1

In Figure 6 we show the first Brodatz texture image that we use in our experiments. The image is slightly unevenly illuminated and has a fairly low contrast, but nevertheless its statistical properties are almost translation invariant.

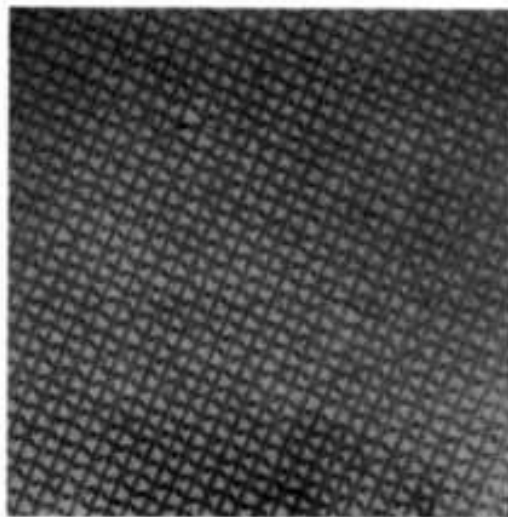


Figure 6: 256×256 image of Brodatz image 1.

In Figure 7 we show the anomaly images that derive from Figure 6. Note

how the anomaly images become smoother as we progress from Figure 7a to Figure 7f, due to the increasing amount of averaging that occurs amongst the overlapping trees in the network.

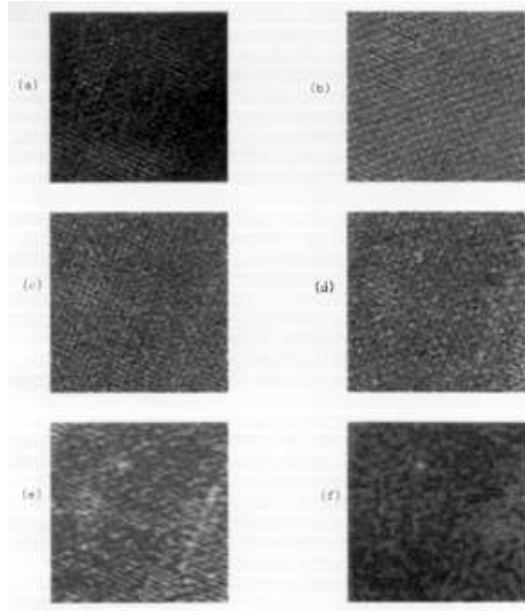


Figure 7: 256×256 anomaly images of Brodatz image 1.

Figure 7e and Figure 7f reveal a highly localised anomaly in the original image. Figure 7f corresponds to a length scale of 8×8 pixels, which is the approximate size of the fault that is about $\frac{1}{4}$ of the way down and slightly to the left of centre of Figure 6. The fault does not show up clearly on the other figures in Figure 7 because their characteristic length scales are either too short or too long to be sensitive to the fault.

From Figure 7 we conclude that ACE can easily pick out localised faults in highly ordered textures.

3.2 Texture 2

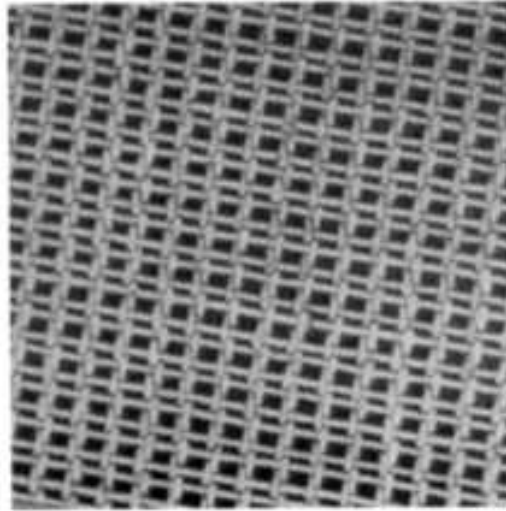


Figure 8: 256×256 image of Brodatz image 2.

In Figure 8 we show the second Brodatz texture image that we use in our experiments. The image has a high contrast and translation invariant statistical properties.

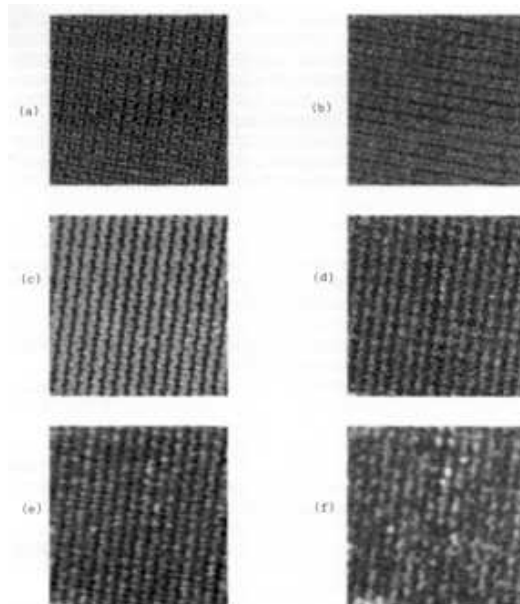


Figure 9: 256×256 anomaly images of Brodatz image 2.

In Figure 9 we show the anomaly images that derive from Figure 8. The most interesting anomaly image is Figure 9f which shows several localised anomalies.

About halfway down and to the left of centre of the image is an anomaly that corresponds to a dark spot on the thread in Figure 8. The brightest of the anomalies in the cluster just above the centre of the image corresponds to what appears to be a slightly torn thread in Figure 8. The other anomalies in this cluster are weaker, and correspond to slight distortions of the threads. There is another anomaly just below and to the right of the centre of Figure 9f, which corresponds to what appears to be another slightly torn thread in Figure 8. These anomalies all occur at, or around, a length scale of 8×8 pixels. Several of the anomaly images show an anomaly in the bottom left hand corner of the image, which corresponds to a small uniform patch of fabric in Figure 8.

The results in Figure 9 corroborate the evidence in Figure 7 that we can train ACE to pick out localised anomalies in highly structured textures. This type of texture could be analysed much more simply by model-based techniques that took advantage of their near-periodicity. However, that does not detract from the fact that, by making use of its adaptability, ACE succeeds in modelling these textures without prior knowledge of their near-periodicity. We seek a general purpose approach to density estimation; not a toolkit of different (usually model-based) techniques, each tuned to its own type of problem.

3.3 Texture 3

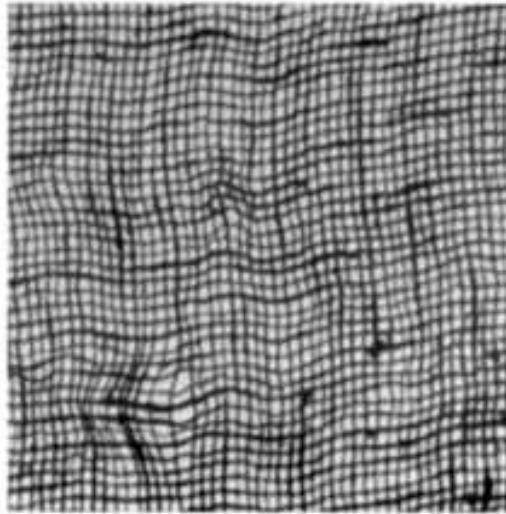


Figure 10: 256×256 image of Brodatz image 3.

In Figure 10 we show the third Brodatz texture image that use in our experiments. The image has a very high contrast and statistical properties that are almost translation invariant. However the density of anomalies is much higher than in either Figure 6 or Figure 8.

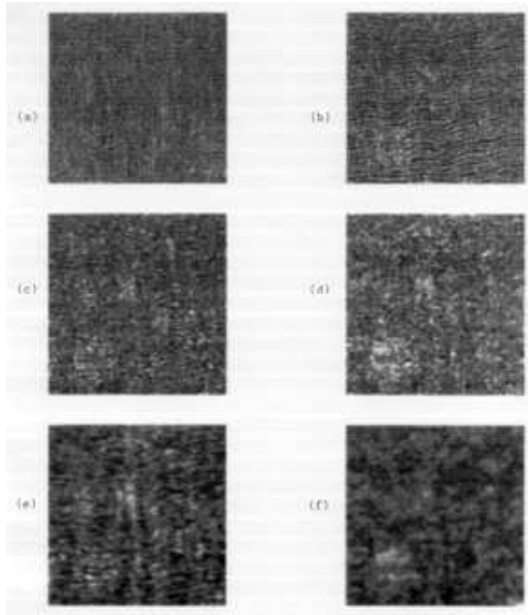


Figure 11: 256×256 anomaly images of Brodatz image 3.

In Figure 11 we show the anomaly images that derive from Figure 10. At the lower left hand corner of Figure 11f there is a large anomaly that corresponds to a region of Figure 10 that is distorted to the left. Figure 11f is sensitive to a length scale of 8×8 pixels, so it does not respond to this leftward distortion (which occurs on a length scale of around 32×32 pixels), rather it responds to localised variations in the separations of the threads.

There are numerous other anomalies in Figure 10; some are detected in Figure 11, and some are not. The ability of ACE to pick out anomalies degrades as the density of anomalies increases. This is because the anomalies themselves are part of the statistical properties that are extracted by ACE from the training image, and if a particular type of anomaly occurs often enough in the image then it is no longer deemed to be an anomaly. In extreme cases there is also the possibility that the entropy (per unit area) of the input image can saturate ACE and thus degrade its performance, as we discussed earlier.

3.4 Texture 4

In this section we present a slightly different type of experiment in which we train ACE on one image and test ACE on another image. To create the two images we start with a single 256×256 image of a Brodatz texture, which we divide into a left half and a right half. We then use the left half to construct a training image, and the right half to construct a test image. Note that in constructing these images we scrupulously avoid the possibility that the training and test images contain elements deriving from a common source, although there are some small residual correlations between the two images along their common edge.

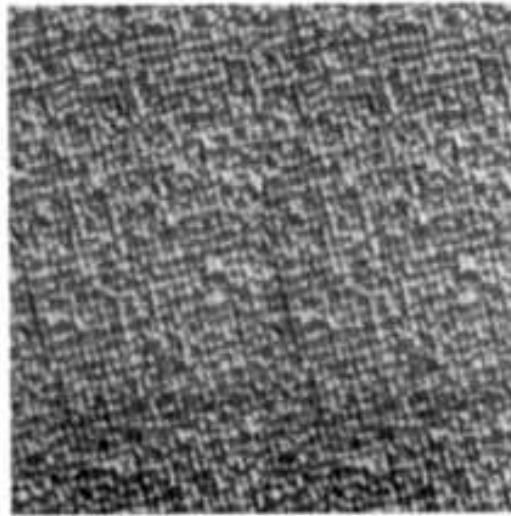


Figure 12: 256×256 image of a Brodatz image of a carpet for training.

In Figure 12 we show the training image which is a montage of two copies of the left hand half of a Brodatz texture image. Note that we use square, rather than rectangular, images because our software is restricted to processing this type of image.

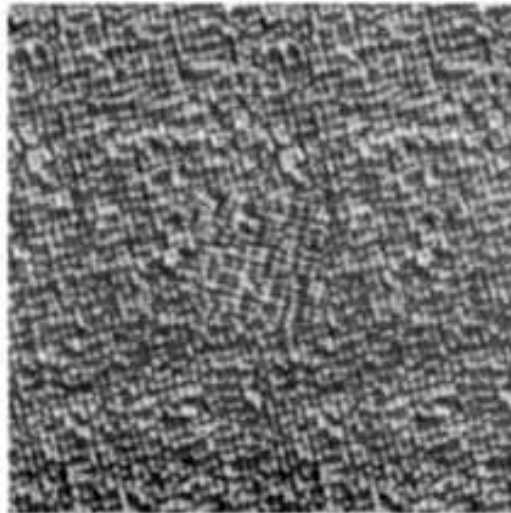


Figure 13: 256×256 image of a Brodatz image of a carpet for testing.

In Figure 13 we show the test image which is a montage of two copies of the right hand half of a Brodatz texture image, and superimposed on that is a 64×64 patch which we generated by flipping the rows and columns of a copy of the top left hand corner of this image. This patch is a hand-crafted anomaly.

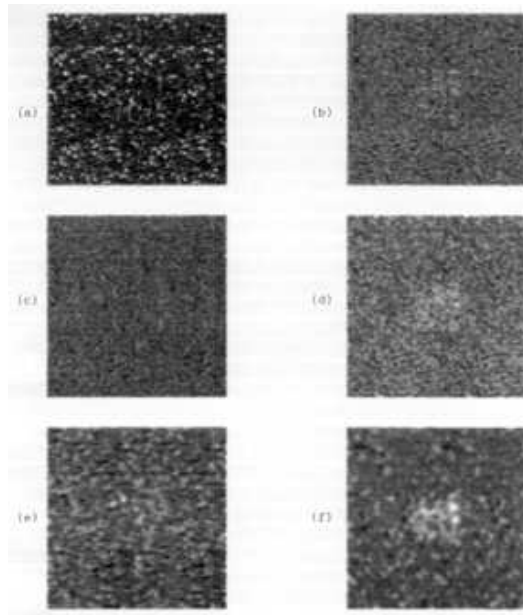


Figure 14: 256×256 anomaly images of a Brodatz image of a carpet.

In Figure 14 we show the anomaly images that derive from Figure 13 after we train on Figure 12. Figure 14f shows the strongest response to the anomalous patch in the centre of the image, corresponding to anomaly detection on a length scale of 8×8 pixels.

4 Conclusions

We present a novel method of density estimation in high-dimensional spaces, such as images. In Bayesian data processing there is a pressing need for a flexible way of constructing such estimates, because the basic objects that we manipulate in Bayesian analysis are joint PDFs, which we must somehow construct in the first place. We call the hierarchical network structure that emerges from our analysis an “Adaptive Cluster Expansion”, or ACE for short.

ACE is computationally very cheap: we can train a multilayer topographic mapping network to estimate the joint PDF of its input data at the rate of 1 network layer every 2.3 second (on a VAXstation 3100, and assuming 6 bits per pixel), where each layer analyses one length scale (power of 2) in the input data. We find, in our experiments with Brodatz textures, that 6 network layers allows the detection of statistical anomalies in the textures. This result is not universal, because it must depend strongly on the scale at which the anomalous statistical structure in the data is to be found. Although we demonstrate ACE only in a texture anomaly detection rôle, its scope is far greater than this. ACE is a general purpose, and computationally cheap, network for estimating densities in high-dimensional spaces.

For completeness, we should mention that the performance of ACE in its current form has two fundamental limitations. Firstly, we assume that the network connectivity is fixed, and that its functionality is determined by a training

algorithm. This restricts the possible statistical properties of the input data that could be estimated. Secondly, ACE is based upon a hierarchically connected multilayer topographic mapping network, which progressively squeezes the input data through an ever smaller bottleneck as we pass through the layers of the network. There is an upper limit to the number of network layers beyond which ACE simply cannot preserve information that is useful in estimating the statistics of the input data. For instance, the statistics of an extremely noisy image of a texture can not be successfully estimated by ACE, because the noise entropy would saturate ACE before the statistics of the underlying texture could be investigated. This problem can be solved by introducing explicit noise models into ACE, which we shall report elsewhere.

A Appendix

The standard topographic mapping training procedure in [7] is a rather inefficient algorithm. In [10] we present in detail an efficient training procedure for topographic mappings, and explain how to use it to train multilayer topographic mappings.

For convenience, we introduce some notation.

\mathbf{x} = input vector

y = index of the winning “neuron”

$\mathbf{x}(y)$ = reference vector associated with y

$\pi(y' - y)$ = topographic neighbourhood function (normalised to unit total mass)

ε = update parameter used during training

N = number of reference vectors

A.1 Standard Topographic Mapping Training Algorithm

The standard topographic mapping training procedure is essentially as follows [7]:

1. Select a training vector \mathbf{x} at random from the training set.
2. Map \mathbf{x} to y by using a nearest neighbour prescription applied to the distance of \mathbf{x} from each of the current set of reference vectors.
3. For all y' , move the reference vector $\mathbf{x}(y')$ directly towards the input vector \mathbf{x} by a distance $\varepsilon \pi(y' - y) \|\mathbf{x} - \mathbf{x}(y')\|$.
4. Go to step 1.

Repeat this loop as often as is required to ensure convergence of the reference vectors.

The standard training method specifies that $\pi(y' - y)$ should be an even unimodal function whose width should be gradually decreased as training progresses. This allows coarse-grained organisation of the reference vectors to occur, followed progressively by ever more fine-grained organisation, until finally the algorithm converges to an optimum set of reference vectors. In a similar vein, the relative size of the update step ε should also be steadily decreased as training progresses.

A.2 Modified Topographic Mapping Training Algorithm

In our own modification [10] of the standard topographic mapping training we replace a shrinking $\pi(y' - y)$ function acting on a fixed number of reference vectors, by a fixed $\pi(y' - y)$ function acting on an increasing number of reference vectors. There are many minor variations on this theme, but we find that it is sufficient to define

$$\pi(y' - y) = \begin{cases} \varepsilon & y' = y \\ \varepsilon' & |y' - y| = 1 \\ 0 & |y' - y| > 1 \end{cases}$$

where we absorb the ε into the definition of $\pi(y' - y)$. We increase the number of reference vectors in a binary sequence (i.e. $N = 2, 4, 8, 16, 32, \dots$), and we initialise each generation of reference vectors by interpolation from the previous generation. We find that the following parameter values yield adequate convergence: $\varepsilon = 0.1$, $\varepsilon' = 0.05$, and we perform $20N$ training updates before doubling the value of N , as above. We initialise the $N = 2$ pair of reference vectors as a random pair of vectors chosen from the training set.

In numerous experiments, we find that this modified form of the topographic mapping training algorithm converges much more rapidly than the standard method. Furthermore, the binary sequence of N values lends itself well to implementing the trained topographic mapping using a look-up table.

References

- [1] R. T. Cox (1946). Probability, frequency and reasonable expectation. *Am. J. Phys.*, **14**(1), 1-13.
- [2] H. Jeffreys (1939). *Theory of Probability* (Clarendon Press, Oxford).
- [3] D. H. Ackley, G. E. Hinton and T. J. Sejnowski (1985). A learning algorithm for Boltzmann machines. *Cognitive Sci.*, **9**(1), 147-169.
- [4] T. J. Sejnowski (1987). Higher order Boltzmann machines. In *Proc. Conf. on Neural networks for Computing (vol. 151)*, (Am. Inst. Phys., Snowbird), 398-403.
- [5] E. T. Jaynes (1982). On the rationale of maximum entropy methods. *Proc. IEEE*, **70**(9), 939-952.
- [6] S. P. Luttrell (1989). The use of Bayesian and entropic methods in neural network theory. In *Maximum Entropy and Bayesian Methods*, edited by G. Erickson, J. T. Rychert and C. R. Smith (Kluwer, Dordrecht), 363-370.
- [7] T. Kohonen (1984). *Self-Organisation and Associative Memory* (Springer-Verlag, Berlin).
- [8] S. P. Luttrell (1989). Image compression using a multilayer neural network. *Patt. Recogn. Lett.*, **10**(1), 1-7.
- [9] S. P. Luttrell (1989). Hierarchical self-organising networks. In *Proc. 1st IEE Conf. on Artificial Neural Networks*, (IEE, London), 2-6.

- [10] S. P. Luttrell (1989). Hierarchical vector quantisation. *Proc. Inst. Electr. Eng. I*, **136**(6), 405-413.
- [11] S. P. Luttrell (1990). Derivation of a class of training algorithms. *IEEE Trans. Neural Networ.*, **1**(2), 229-232.
- [12] S. P. Luttrell (1991). Self-supervised training of hierarchical vector quantisers. In *Proc. 2nd IEE Conf. on Artificial Neural Networks*, (IEE, London), 5-9.
- [13] P. Brodatz (1966). *Textures - A Photographic Album for Artists and Designers* (Dover, New York).